

forming ICP/EDS, TGA, and N₂ adsorption–desorption isotherm measurements, respectively. XANES data were collected in transmission mode at beam line 7C at the Pohang Light Source (Pohang, Korea).

Received: March 28, 2005

Final version: June 30, 2005

Published online: October 11, 2005

- [1] Y. Xia, P. Yang, Y. Sun, Y. Wu, B. Mayers, B. Gates, Y. Yin, F. Kim, H. Yan, *Adv. Mater.* **2003**, *15*, 353.
- [2] a) M. S. Whittingham, *Chem. Rev.* **2004**, *10*, 4271. b) M. M. Thackeray, *Prog. Solid State Chem.* **1997**, *25*, 1. c) S.-J. Hwang, H. S. Park, J. H. Choy, G. Campet, *J. Phys. Chem. B* **2000**, *104*, 7612.
- [3] a) J. Kim, A. Manthiram, *Nature* **1997**, *390*, 265. b) S.-J. Hwang, C. W. Kwon, J. Portier, G. Campet, H. S. Park, J. H. Choy, P. V. Huang, M. Yoshimura, M. Kakihana, *J. Phys. Chem. B* **2002**, *106*, 4053.
- [4] a) Y. Zhou, C. Shen, J. Huang, H. Li, *Mater. Sci. Eng., B* **2002**, *95*, 77. b) Y. Zhou, J. Huang, C. Shen, H. Li, *Mater. Sci. Eng., A* **2002**, *335*, 260. c) Y. Zhou, C. Shen, H. Li, *Solid State Ionics* **2002**, *146*, 81.
- [5] a) X. Wang, Y. Li, *J. Am. Chem. Soc.* **2002**, *124*, 2880. b) R. Ma, Y. Bando, L. Zang, T. Sasaki, *Adv. Mater.* **2004**, *16*, 918. c) X. Wang, Y. Li, *Chem. Eur. J.* **2003**, *9*, 300. d) X. Wang, Y. Li, *Chem. Lett.* **2004**, *33*, 48.
- [6] a) Z. Lu, D. D. MacNeil, J. R. Dahn, *Electrochem. Solid-State Lett.* **2001**, *4*, A191. b) X. Wang, F. Zhou, X. Zhao, Z. Zhang, M. Ji, C. Tang, T. Shen, H. Zheng, *J. Cryst. Growth* **2004**, *267*, 184.
- [7] Lattice parameters: $a = 2.894 \text{ \AA}$, $c = 14.306 \text{ \AA}$ for the LiMn_{0.5}Ni_{0.5}O₂ precursor; $a = 2.848 \text{ \AA}$, $c = 14.373 \text{ \AA}$ for Li_xMn_{0.67}Ni_{0.33}O₂ nanowires prepared with 0.5 M persulfate solution.
- [8] B. Douglas, D. McDaniel, J. Alexander, *Concepts and Models of Inorganic Chemistry*, 3rd ed., Wiley, New York **1993**, p. E-3.
- [9] Light elements like lithium cannot be detected by EDS analysis.
- [10] G. R. Patzke, F. Krumeich, R. Nesper, *Angew. Chem. Int. Ed.* **2002**, *41*, 2446.

Patterned MoS₂ Nanostructures Over Centimeter-Square Areas**

By Christopher L. Stender, Eric C. Greyson, Yelizaveta Babayan, and Teri W. Odom*

This paper reports an approach for the generation of molybdenum disulfide nanostructures by the sulfidation of patterned sub-300 nm features of molybdenum metal. Our method can be used to pattern arbitrary shapes of MoS₂ nanostructures with independent control over their width, height,

and length. In addition, we can control the orientation of the crystals by placing the patterned substrates at different locations in the quartz tube furnace. These nanostructures can be fabricated with variable pitch, over large areas (cm²), and on a range of insulating and conducting substrates (e.g., sapphire, fused silica, and silicon). This work provides a general strategy for patterning nanoscale crystalline structures on surfaces—in particular, metal sulfide nanomaterials—by combining top-down nanoscale patterning techniques with bottom-up chemical methods.

MoS₂ is a layered semiconducting material that has shown promise in chemical sensors,^[1] in solar cells,^[2] in catalysis,^[3–5] and for low-friction surfaces.^[6–8] Recent studies have suggested that reducing the size of the MoS₂ crystals can improve their lubrication properties in bearings, O-rings, or other heavy-wear applications.^[9] The ability to pattern MoS₂ nanostructures and other metal-sulfide materials on surfaces with specific sizes and shapes has the potential to optimize and improve their usefulness. MoS₂ ribbons have successfully been grown on the step edges of highly oriented pyrolytic graphite by electrochemical methods.^[10,11] Although the heating of MoO₂ nanowires in H₂S for several days could achieve increased lateral dimensions of MoS₂ ribbons, control of other aspects of this system, such as the height, the spacing, and the overall length of the ribbons, remains a challenge.

There are two strategies for organizing nanostructures on surfaces: i) synthesis of the nanomaterials followed by assembly into architectures, or ii) direct growth of the nanostructures at predefined locations. The former approach relies on assembly methods such as fluidic-based assembly,^[12,13] electric- and magnetic-field-mediated assembly,^[14–16] electrostatic assembly,^[17,18] and template-based assembly.^[19,20] Serial lithographic techniques, including scanning-probe and electron-beam (e-beam) writing, can easily pattern functional structures with sub-100 nm features; however, their slow write speeds and small write areas can be a drawback.^[21–23] Examples of parallel patterning methods are nanosphere lithography and laser-assisted embossing, which can generate sub-100 nm patterns of simple geometries.^[24,25] We and others have developed a suite of soft-lithographic nanopatterning tools that can generate small (sub-30 nm) features over relatively large areas (>1 cm²) in a parallel process.^[26,27] These tools have been used to create Si and GaAs nanostructures by chemical etching^[28,29] and to direct the growth of arrays of ZnO nanowires and carbon nanotubes.^[30–32] Here we report an important variant of the directed-growth method: instead of using the lithographically patterned metallic areas to nucleate and/or catalyze the growth of nanostructures, we are *chemically converting* the nanopatterns into crystalline nanostructures. We can thus accomplish the organization of nanomaterials over centimeter-square areas by using soft-lithographic nanopatterning and can achieve functional materials by simple sulfidation reactions.

Figure 1 outlines the procedure for patterning MoS₂ nanostructures. First, phase-shifting photolithography was used to generate sub-300 nm trenches in negative-tone photoresist.^[27]

[*] Prof. T. W. Odom, C. L. Stender, E. C. Greyson, Y. Babayan
Department of Chemistry, Northwestern University
2145 Sheridan Road, Evanston, IL 60208 (USA)
E-mail: todom@northwestern.edu

[**] This research was supported by an NSF CAREER Award (CHE-0349302). This work made use of the NUANCE Center facilities, which are supported by NSF-MRSEC, NSF-NSEC, Keck Foundation and Northwestern University. Supporting Information is available online from Wiley InterScience or from the author.

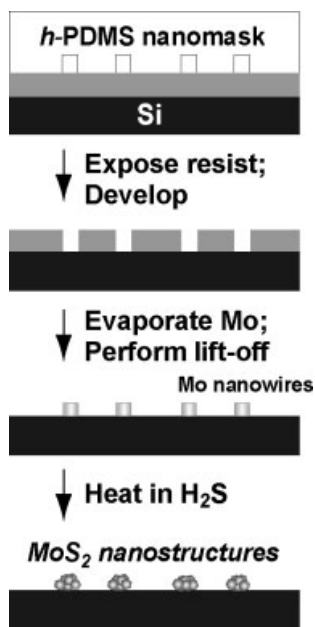


Figure 1. Schematic diagram outlining the procedure for patterning MoS₂ nanostructures; h-PDMS: hard poly(dimethylsiloxane).

We then deposited, by electron-beam (e-beam) deposition, a thin (<5 nm) Cr adhesion layer followed by 25–90 nm of Mo onto the patterned substrates. After removal of the photoresist, we placed the Mo patterns into a quartz-tube furnace (13 in. in length, 1 in. = 2.54 cm) for sulfidation. The temperature was slowly ramped (2 °C min⁻¹) to 850 °C under a flow of Ar and H₂S gas; the sample was held at this temperature for 4 h. These reaction conditions are similar to previous studies

that used H₂S gas as the sulfur source for the conversion of MoO₂/O₃ to MoS₂. Notably, our reaction times are significantly shorter (4 h compared to 24–84 h).^[10,11,33]

Field-emission scanning electron microscopy (FE-SEM) images of patterned Mo lines 90 nm in height (90 nm Mo lines) and the MoS₂ lines obtained after sulfidation are shown in Figures 2A–C. The MoS₂ nanostructures in Figures 2B,C are morphologically distinct from each other. The former image depicts crystals that overlap and are oriented parallel to the silicon substrate, while the latter image shows crystals that are oriented perpendicular to the substrate. What is interesting is that the patterned Mo lines were subjected to identical reaction conditions (gases, temperatures) except for their *position* inside the tube furnace. Samples placed 9–10” downstream from the entrance formed MoS₂ plates parallel to the substrate (200 nm in height), while samples 3–4” downstream produced MoS₂ plates oriented nearly perpendicular to the substrate (50–150 nm thickness on the edge).

To investigate how the conversion of Mo to MoS₂ depended on the thickness of the initial Mo layer, we reacted patterns of 25 nm tall Mo lines (Fig. 2D) with H₂S in the furnace. SEM images reveal that the preferential orientations of MoS₂ crystals formed 9–10” downstream from the entrance of the furnace (Fig. 2E) or 3–4” downstream (Fig. 2F) are similar to the MoS₂ nanoplates formed from the 90 nm Mo patterns. Although the general morphological trends are the same for 90 nm and 25 nm samples (downstream MoS₂ nanoplates are oriented parallel to the surface), there are two distinct differences in the sizes of the MoS₂ nanocrystals: i) the MoS₂ crystals formed from the 25 nm Mo samples that lie parallel to the surface do not overlap significantly with neighboring crystals; and ii) the thicknesses of the crystals oriented perpendicular to the surface are reduced substantially. Measured from

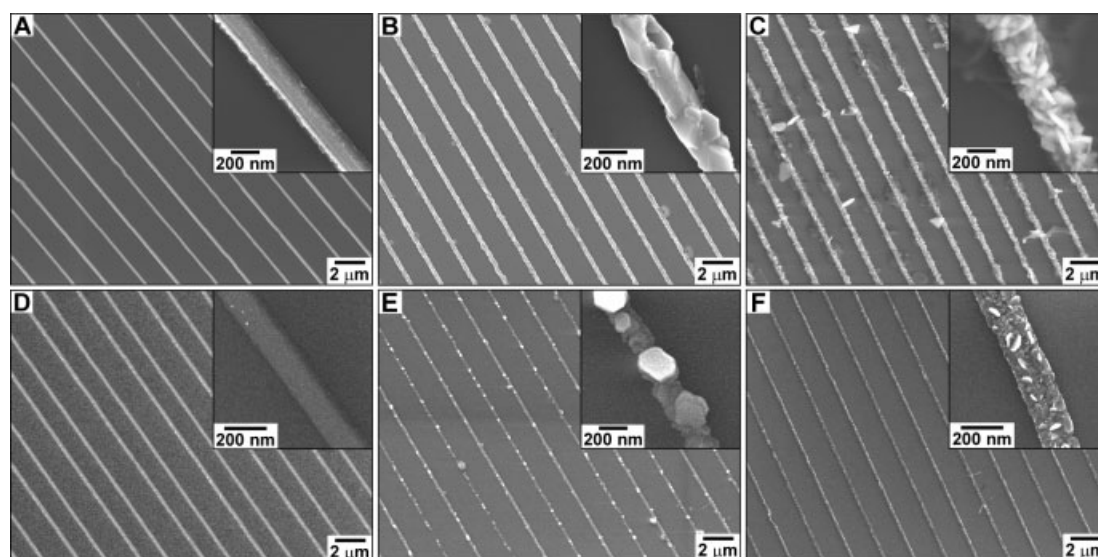


Figure 2. SEM images of lines of as-deposited Mo and MoS₂. A) 90 nm tall Mo lines. B) MoS₂ lines converted from (A) after reacting with H₂S gas. The nanoplates are oriented parallel to the surface and overlap with each other. C) MoS₂ lines converted from (A) with crystals oriented perpendicular to the surface. D) 25 nm tall Mo lines. E) MoS₂ lines converted from (D) placed far downstream of the tube furnace entrance. F) MoS₂ lines converted from (D) placed near the entrance of the tube furnace.

SEM images, the MoS₂ nanoplates parallel to the surface had widths ranging from 100 to 200 nm, and the plates perpendicular to the surface had edge thicknesses of 5–15 nm. We propose that variations in the H₂S concentration along the tube furnace or the decomposition of H₂S gas along the length of the furnace contribute to the preferential orientation of MoS₂ nanocrystals.

We characterized the chemical composition of as-deposited Mo films to improve our understanding of how the nanopatterned Mo lines converted to MoS₂ nanostructures. Upon their removal from the e-beam evaporator, the samples were immediately exposed to oxygen (from ambient conditions), and during their heating in H₂S ($P_{\text{H}_2\text{S}} \sim 70$ torr, $P_{\text{Ar}} \sim 690$ torr; P = pressure, 1 torr \approx 133 Pa), there were small amounts ($P_{\text{O}_2} \sim 3 \times 10^{-4}$ torr) of oxygen present. We verified the presence of MoO_x (mixture of Mo/MoO₂) in the patterned Mo lines using X-ray photoelectron spectroscopy (XPS) (see Supporting Information). We propose two possible mechanisms for the sulfidation of our as-deposited Mo metal nanopatterns: i) conversion of the MoO_x present in the patterns to MoS₂ crystalline nanostructures^[11] and/or ii) direct sulfidation of the Mo metal nanopatterns.^[34] For both mechanisms, there is a limited range over which the reaction conditions are optimal. We found that at higher temperatures (> 900 °C) and/or longer reaction times (> 12 h), the silicon substrate and the Mo patterns degrade; at lower temperatures (< 800 °C) and/or shorter times (< 4 h) the Mo patterns were neither fully converted to MoS₂ nor highly crystalline.

One advantage of our nanopatterning followed by chemical conversion method is that nanostructures that differ from straight lines can be generated. Figure 3 demonstrates that our technique can be used to pattern individual, 300 nm diameter MoS₂ dots, as well as curved nanostructures. The MoS₂ dots highlight that crystalline structures can be formed directly from amorphous Mo/MoO_x materials. Interestingly, when the lateral size of the Mo patterns becomes larger than 300 nm, the MoS₂ nanocrystals do not exhibit the dramatic orientational preference depending on their growth position in the furnace. MoS₂ films and patterned microstructures consisted of a mixture of crystals oriented parallel and perpendicular to the substrate.

Powder X-ray diffraction (PXRD) spectra of patterned MoS₂ nanostructures and MoS₂ nanostructured films are consistent with bulk 3R-MoS₂ (Powder Diffraction File, PDF #00-017-0744) comprised of Mo atoms trigonally coordinated with S atoms in a sandwich arrangement with three layers per unit cell. Because of the different orientations of the MoS₂ nanocrystals in the nanocrystalline films, certain peaks are exaggerated in the PXRD spectrum. For example, the (003) peak is very small in films when a majority of the plates are oriented normal to the surface (Fig. 4A); MoS₂ films with a higher percentage of plates parallel to the surface exhibit the (003) peak (Fig. 4B). Patterned MoS₂ lines possessing crystals oriented parallel to the substrate show only a weak, single (003) peak. In most of the diffraction patterns, a large peak near $2\theta = 15.9^\circ$ is observed. It is possible that this peak is from

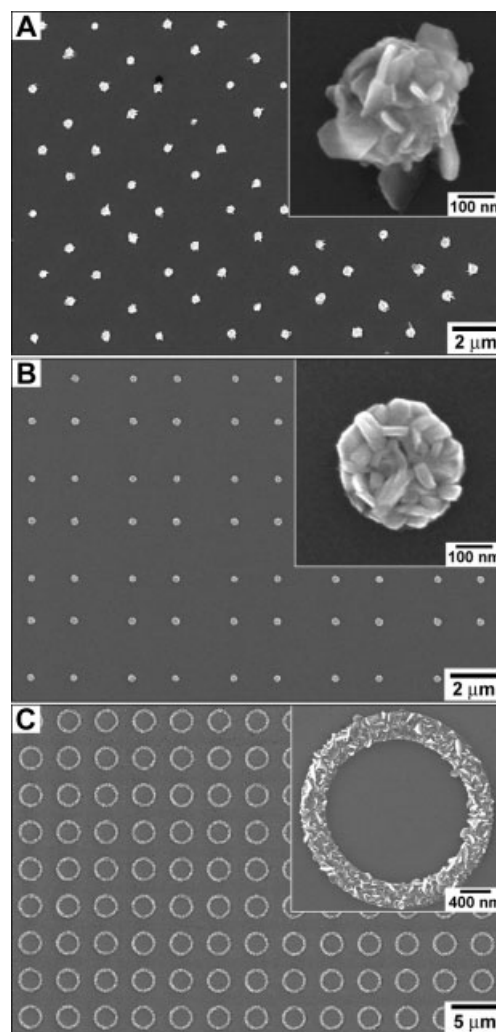


Figure 3. SEM images of A) MoS₂ dots converted from 90 nm tall Mo dots, and B) 25 nm tall Mo dots. C) Rings of MoS₂ nanostructures illustrate our ability to form crystals on curved patterns.

a Cr₂S₃ layer (PDF # 03-065-4651), which forms when the underlying Cr adhesion layer reacts with the H₂S, since our reaction conditions are similar to those used to synthesize Cr₂S₃.^[35]

We measured the optical properties of MoS₂ nanostructures on quartz substrates by UV-vis absorption spectroscopy. Figure 5 shows two distinct absorption maxima corresponding to the A1 and B1 exciton peaks in crystalline MoS₂.^[11,36] The position of the peaks for MoS₂ films formed by sulfidation of the 25 nm Mo and 90 nm Mo films were nearly identical (within 5 nm).

In summary, we have demonstrated how soft-lithographic techniques can be used to generate patterns of MoS₂ nanostructures with controllable orientation, height, width, and shape. Limitations of our strategy include: i) supporting surfaces for the nanostructures need to be stable at high temperatures (850 °C), and ii) toxicity of the sulfur source. Since most technologically relevant surfaces (e.g., Si, SiO₂, and

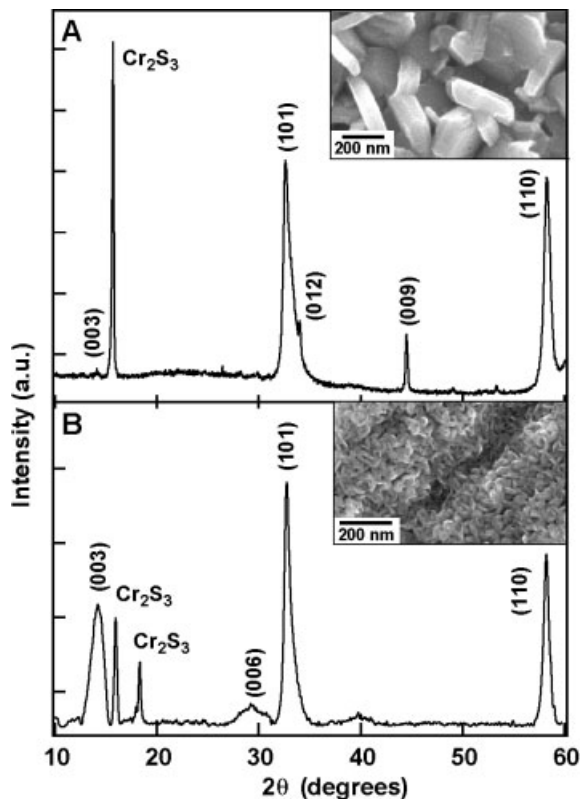


Figure 4. PXRD patterns of MoS₂ nanostructured films where the majority of the nanoplates were oriented A) nearly perpendicular to the substrate, and B) mostly parallel to the substrate. Insets depict portions of the MoS₂ nanostructured films. The contributions of the Cr₂S₃ underlayer to the PXRD patterns are indicated, and the large intensity of the MoS₂ (009) peak in (A) most likely is from the (11-6) peak of Cr₂S₃.

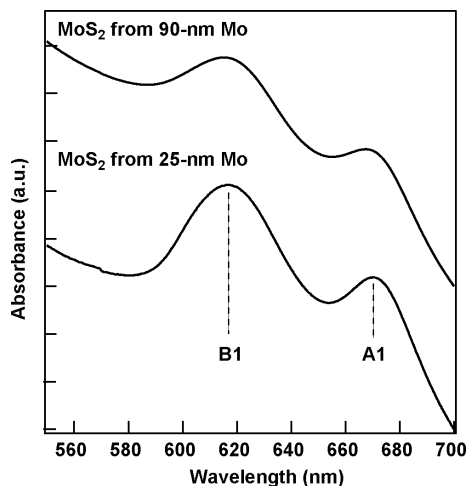


Figure 5. UV-vis absorption spectroscopy of MoS₂ nanostructured films converted from Mo films that were 90 and 25 nm thick. The positions of the two exciton peaks, A1 and B1, are indicated by dashed lines.

GaAs) can withstand such temperatures, this drawback is minimized. Also, careful gas-handling and proper exhaust equipment can alleviate concerns about H₂S. These patterning

methods, moreover, offer a general approach to create patterned metal oxide and chalcogenide nanostructures on surfaces, which can be integrated directly into device platforms. Our ability to control the orientation of the MoS₂ nanocrystals may also be important in applications such as catalysis and sensors, which become more effective with the increased surface area of materials.

Experimental

Fabrication of Arrays of Molybdenum Nanostructures: Phase-shifting photolithography (PSP) was used to generate sub-300 nm trenches in negative-tone photoresist (Microposit ma-405) by exposing broadband UV light (365–436 nm) through *h*-PDMS (hard poly(dimethylsiloxane)) masks patterned with recessed features (lines, rings, or dots). The features in the *h*-PDMS mask were ~200 nm in width (smallest was 100 nm; largest was ~300 nm) and 400 nm in height. Instead of producing features at the *edges* of the mask, which is typically observed in standard PSP, the nanopatterned mask generated features in negative photoresist that were *identical* in size and pitch to the *h*-PDMS mask [27]. We then used an e-beam to deposit a thin (<5 nm) Cr adhesion layer followed by 25–90 nm of Mo onto the patterned substrates. The photoresist was removed by agitation in acetone and organic solvents.

Chemical Conversion of Molybdenum Nanopatterns: Silicon substrates patterned with Mo lines, rings and dots were placed in a 2" diameter (13" length) tube furnace. Oxygen was purged from the system by five consecutive cycles of pumping down to ~20 torr and refilling with 99.99% Ar gas. The temperature was slowly ramped (2°C min⁻¹) to 850 °C under a flow of Ar (200 sccm, P_{Ar} ~690 torr) and H₂S gas (20 sccm, P_{H₂S} ~70 torr); samples were held at this temperature for 4 h. After 4 h, the chamber was purged for 20 min. with Ar gas (1500 sccm) and allowed to cool to ambient temperature over a 90 min period.

Characterization of MoS₂ Nanostructures: FE-SEM images were obtained on a LEO 1525 microscope. PXRD spectra were measured using a Rigaku D/MAX 8 X-ray diffractometer. XPS spectra were taken using an Omicron ESCA Probe X-ray photoelectron spectrometer.

Received: April 25, 2005
Final version: June 28, 2005
Published online: October 11, 2005

- [1] H. Zhang, K. P. Loh, C. H. Sow, H. Gu, X. Su, C. Huang, Z. K. Chen, *Langmuir* **2004**, *20*, 6914.
- [2] N. Barreau, J. C. Bernede, *J. Phys. D: Appl. Phys.* **2002**, *35*, 1197.
- [3] J. P. Wilcoxon, *J. Phys. Chem. B.* **2000**, *104*, 7334.
- [4] W. Ho, J. C. Yu, J. Lin, J. Yu, P. Li, *Langmuir* **2004**, *20*, 5865.
- [5] M. Kouzu, K. Uchida, Y. Kuriki, F. Ikazaki, *Appl. Catal., A* **2004**, *276*, 241.
- [6] S. H. Loewenthal, R. G. Chou, G. B. Hopple, W. L. Wenger, *Tribol. Trans.* **1994**, *37*, 505.
- [7] I. L. Singer, S. Fayeulle, P. D. Ehni, *Wear* **1996**, *195*, 7.
- [8] I. M. Pavlov, L. F. Shevakin, L. S. Seidaliev, *Wear* **1960**, *3*, 406.
- [9] L. Rapoport, Y. Bilik, Y. Feldman, M. Homyonfer, S. R. Cohen, R. Tenne, *Nature* **1997**, *387*, 791.
- [10] Q. Li, J. T. Newberg, E. C. Walter, J. C. Hemminger, R. M. Penner, *Nano Lett.* **2004**, *4*, 277.
- [11] Q. Li, E. C. Walter, W. E. van der Veer, B. J. Murrey, J. T. Newberg, E. W. Bohannon, J. A. Switzer, J. C. Hemminger, R. M. Penner, *J. Phys. Chem. B.* **2005**, *109*, 3169.
- [12] F. Kim, S. Kwan, J. Akana, P. Yang, *J. Am. Chem. Soc.* **2001**, *123*, 4360.
- [13] Y. Huang, X. Duan, Q. Wei, C. M. Lieber, *Science* **2001**, *291*, 630.

- [14] A. S. Smith, C. D. Nordquist, T. N. Jackson, T. S. Mayer, B. R. Martin, J. K. N. Mbindyo, T. E. Mallouk, *Appl. Phys. Lett.* **2000**, *77*, 1399.
- [15] X. Duan, Y. Huang, Y. Cui, J. Wang, C. M. Leiber, *Nature* **2001**, *409*, 66.
- [16] H. Zhang, S. Boussaad, N. Ly, N. J. Tao, *Appl. Phys. Lett.* **2004**, *84*, 133.
- [17] Z. Tang, N. A. Kotov, M. Giersig, *Science* **2002**, *297*, 237.
- [18] S. C. Kuiry, S. D. Patil, S. Deshpande, S. Seal, *J. Phys. Chem. B* **2005**, *109*, 6936.
- [19] Y. A. Vlasov, N. Yao, D. J. Norris, *Adv. Mater.* **1999**, *11*, 165.
- [20] Y. Yin, Y. Lu, B. Gates, Y. Xia, *J. Am. Chem. Soc.* **2001**, *123*, 8718.
- [21] R. Steffen, J. Oshinowo, T. Koch, A. Forchel, *J. Vac. Sci. Technol., B* **1995**, *13*, 2888.
- [22] H. Zhang, C. A. Mirkin, *Chem. Mater.* **2004**, *16*, 1480.
- [23] P. R. Krauss, S. Y. Chou, *J. Vac. Sci. Technol., B* **2005**, *13*, 2850.
- [24] J. C. Hultheen, R. P. V. Duyne, *J. Vac. Sci. Technol., B* **1995**, *13*, 1553.
- [25] J. E. Barton, T. W. Odom, *Nano Lett.* **2004**, *4*, 1525.
- [26] T. W. Odom, J. C. Love, D. B. Wolfe, K. E. Paul, G. M. Whitesides, *Langmuir* **2002**, *18*, 5314.
- [27] T. W. Odom, V. R. Thalladi, J. C. Love, G. M. Whitesides, *J. Am. Chem. Soc.* **2002**, *124*, 12112.
- [28] Y. Yin, B. Gates, Y. Xia, *Adv. Mater.* **2000**, *12*, 1426.
- [29] Y. Sun, D. Y. Khang, F. Hua, K. Hurley, R. G. Nuzzo, J. A. Rogers, *Adv. Funct. Mater.* **2005**, *15*, 30.
- [30] J. Kong, H. T. Soh, A. M. Cassell, C. F. Quate, H. Dai, *Nature* **1998**, *395*, 878.
- [31] M. H. Huang, S. Mao, H. Feich, H. Yang, Y. Wu, H. Kind, E. Weber, R. Russo, P. Yang, *Science* **2001**, *292*, 1897.
- [32] E. C. Greyson, Y. Babayan, T. W. Odom, *Adv. Mater.* **2004**, *16*, 1348.
- [33] L. Margulis, G. Salitra, R. Tenne, M. Talianker, *Nature* **1993**, *365*, 113.
- [34] B. S. Lee, R. A. Rapp, *J. Electrochem. Soc.* **1984**, *131*, 2998.
- [35] J. Ge, J. Wang, H. Zhang, Y. Li, *Chem. Eur. J.* **2004**, *10*, 3525.
- [36] A. Clark, R. H. Williams, *Br. J. Appl. Phys.* **1968**, *1*, 1222.

Efficient Organic Heterojunction Photovoltaic Cells Based on Triplet Materials**

By Yan Shao and Yang Yang*

Much effort has been expended during the past two decades in the search for organic photovoltaic materials and related device architectures since the donor–acceptor heterojunction interface was demonstrated to be an effective exciton-dissociation structure.^[1–8] The effective organic photovoltaic materials include small molecules and polymers with relatively

high conductivity or mobility. The power-conversion efficiencies of organic photovoltaic devices are dependent on three key processes: light absorption, exciton dissociation, and charge collection.^[4] The external quantum efficiency can be estimated as $\gamma_{\text{total}} = \gamma_{\text{absorption}}\gamma_{\text{dissociation}}\gamma_{\text{collection}}$, where γ_{total} stands for total external quantum efficiency, $\gamma_{\text{absorption}}$ for light absorption, $\gamma_{\text{dissociation}}$ for exciton dissociation, and $\gamma_{\text{collection}}$ for electrode collection.

To gain high power-conversion efficiency, firstly, organic layers should be thick enough to ensure high light absorption, even though many organic photovoltaic materials possess better light-absorption capabilities compared with their inorganic counterparts with similar bandgap and thickness. However, due to the poor exciton mobility, the organic layer in the device has to be sufficiently thin, allowing the photogenerated excitons to reach the junction. In other words, their exciton diffusion lengths cannot match the respective optical absorption lengths.^[3] The exciton diffusion length is dependent on two factors: exciton mobility and lifetime.^[5] In order to improve exciton diffusion length we can adopt high-mobility organics, as has been demonstrated for many high-performance photovoltaic devices,^[2,6,8] or, on the other hand, we can introduce materials with long exciton lifetimes. In this case, triplet materials might be excellent candidates as they often possess much longer exciton lifetimes compared with singlet ones. Fullerenes (C₆₀) are one of the best acceptor materials for organic photovoltaics owing to excellent exciton mobility, a relatively stable triplet state, and, therefore, a relatively large exciton diffusion length,^[9,10] which has been reported to be as long as 400 Å.^[3] Combined with its high electron affinity (EA), C₆₀ and its derivatives have received much attention and have been adopted extensively in organic solar cells.^[2,5,6,8]

There are two general types of organic photovoltaic structure: heterojunctions and bulk heterojunctions (or so-called interpenetrating network structures for the case of polymer blends), which provide respective advantages. Heterojunction devices often have multilayer structures and are formed by layer-by-layer material deposition. Bulk heterojunctions are fabricated via blending or codeposition methods.^[11,12] The interpenetrating networks have proven to be very efficient exciton-dissociation systems, especially for recently reported high-efficiency polymer-based devices.^[5] The exciton- and charge-transport properties are altered after the formation of bulk heterojunctions, since phase separation and film morphology play more important roles compared to in the respective pure materials, so that the mixtures might be considered as whole systems and their properties must be determined after fabrication.^[10,13] On the other hand, heterojunctions are relatively simple systems and the transport properties, crystalline order, and film morphology can be preserved relatively well. Therefore, materials can be characterized independently before device fabrication and the different components can be substituted conveniently. Many valuable parameters can be determined experimentally in heterojunction systems.^[3] In this case, heterojunctions are well suited to the investigation of new materials and theoretical approaches for photovoltaic devices.^[7,11,14]

[*] Prof. Yang Yang, Yan Shao
Department of Materials Science and Engineering
University of California, Los Angeles
Los Angeles, CA 90095 (USA)
E-mail: yangy@ucla.edu

[**] The authors acknowledge financial support from the Office of Naval Research (N00014-04-1-0434) and technical discussion with Douglas Sievers, W.-J. Hou, Dr. Gang Li, and Ankita Prakash.